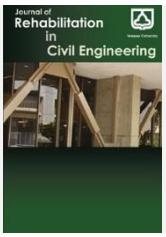

Journal of Rehabilitation in Civil Engineering

Journal homepage: https://civiljournal.semnan.ac.ir/

Numerical Study of the Effect of Transverse Reinforcement on Compressive Strength and Load-Bearing Capacity of Elliptical CFDST Columns

Ali Mohammad Ali[1*]; Sima Besharat Ferdosi[2]; Laith Kareem Obeas[3]; Alwaleed Khalid Ghalib[4]; Meisam Porbashiri[5]

1. Technical Institute of Babylon, AL-Furate AL-Awsat Technical University (ATU), Iraq
2. Department of Mechanical Engineering, Lamar University, Beaumont, Texas, United States
3. Technical Institute of Babylon, AL - Furate AL - Awsat Technical University (ATU), Iraq
4. Chemical Engineer, Thiqar Oil Company, Iraq
5. Department of Mechanical Engineering, Ferdowsi University of Mashhad, Mashhad, Iran

* Corresponding author: *Laith 1978@atu.edu.iq*

ARTICLE INFO

Article history:
Received: 02 December 2022
Revised: 31 May 2023
Accepted: 05 July 2023

Keywords:
CFSDT column,
Buckling behavior,
Abaqus software,
Elliptical column,
Transverse reinforcement.

ABSTRACT

During this research, the buckling behavior of elliptical CDFST columns is investigated numerically in Abaqus Software using transverse reinforcements in the outer tube of the column. For this purpose, an elliptical CFDST column is simulated in Abaqus Software and subjected to compressive loading. The transverse reinforcements are validated and placed in the outer tube of the elliptical CFDST column, and parameters such as thickness, reinforcement dimensions, and distance between them vary within the range of 4, 6, 8 mm; 2, 4, 6 cm, and 2, 4 and 6 cm, respectively and a total of 27 models will be analyzed during the research. The results obtained from this study are in good agreement with the results of previous studies and showed that the finite element method can provide accurate behavior of these columns. The results of this study showed a 15 to 40% increase in load-bearing capacity with the highest compressive strength in elliptical CFDST columns using transverse reinforcements. Also, the effect of increasing the thickness and dimensions on load bearing enhances by 20% and 15%, respectively while the effect of increasing the distance between transverse reinforcements reduces the bearing capacity by 10%. The maximum axial strength was observed in CFDST columns with transverse reinforcements.

E-ISSN: 2345-4423

How to cite this article:
Mohammed Ali, A., Besharat Ferdosi, S., Kareem Obeas, L., Khalid Ghalib, A. and Porbashiri, M. (2024). Numerical study of the effect of transverse reinforcement on compressive strength and load-bearing capacity of elliptical CFDST columns. Journal of Rehabilitation in Civil Engineering, 12(1), 106-126. https://doi.org/10.22075/jrce.2023.29167.1764

1. Introduction

The concept of CFDST was first introduced in underwater pressure vessels, which required high flexural stiffness to prevent instability under external pressures. CFDST columns have excellent structural performance in terms of strength, ductility, and fire resistance [1–3]. These columns have excellent resistance to seismic loads with lower weight and higher fire resistance compared to CFT columns in an equal cross-sectional area [4–7]. The ultimate strength of a CFDST column depends on the compressive strength of concrete, concrete confinement pressure, yield strength of steel tubes, and the ratio of diameter to thickness of internal and external tubes [5,8]. These columns have the advantage of both steel and concrete at the same time. However, the strength of these columns can be reduced by using high-strength steel and concrete, which increases the use of more building space [4].

These columns are also used for nuclear shelters, hazardous liquids and gases storage areas, and explosion-proof spaces. These columns were used in high stairs in Japan due to their good damping properties, high energy absorption, and equivalent cross-sectional area with a lower weight. Also, these columns have found many applications in corridors and high spaces with open spans and buildings [1,4,9].

In CFT columns, the central part of the concrete core has a negligible contribution to flexural and torsional strength. By removing the central part of the concrete and replacing it with a steel tube, the CFDST column's strength increased in comparison to the CFT. This is done by reducing the weight of the column and increasing its strength through the inner tube's confinement pressure [2].

Various experimental and numerical studies have been performed on CFDST columns which have examined different geometries such as circular, square, elliptical, and hybrid geometries which are shown in Figure 1.

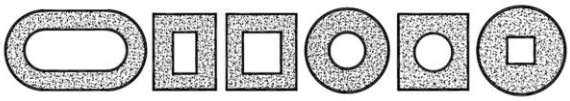

Fig 1. Schematic of CFDST columns with different sections [3].

The behavior of the stress-strain curve of a concrete-filled-steel-tube column was investigated by Chen et al. [7]. They studied the path-dependent stress-strain model for CFST columns, which consists of four components: an interaction model, an accurate hoop strain model, a modified axial stress-strain model of passively confined concrete, and a three-dimensional stress-strain relationship of steel tubes. They obtained that the proposed hoop strain model, passively confined concrete axial stress-strain curve, three-dimensional stress-strain model of HST, and the interaction model between HST and concrete considering de-bonding effect can accurately predict axial load-strain curves of CFST columns. The performance of CFDST columns using stainless steel in outer tubes was investigated by Le et al. [10]. They presented the numerical analysis and design of rectangular CFDST short columns with outer stainless-steel tubes. A finite element model is created to account for the confinement mechanism of concrete, strain hardening of stainless steel, and imperfection of steel tubes. Results illustrated that Circular CFDST columns have a greater lateral confinement effect and higher ultimate load capacity than square CFDST columns. Thick-walled inner carbon steel is employed to ensure the required ductility. Ye et al. [11]. In 2020, studied the mechanical behavior of CFSST members subjected to concentric tension using FEA modeling. Results showed that the steel ratio and 0.2% proof stress of stainless steel are the two primary parameters that determine the ultimate tensile strength of CFSST members. A calculation model is proposed to predict the ultimate strength of CFSST members with acceptable agreements and numerical results. Li et al. [12] investigated the post-buckling

behavior and residual capacity of CFDST columns exposed to explosive loads. In their research, they presented a numerical model to investigate the explosive behavior in these columns and provided a formula for quickly calculating the residual axial capacity in these columns under explosive load [13].

CFT columns with recycled concrete were studied by Xu et al [14]. They presented a set of data mining analyses on the structural performance of recycled aggregate concrete-filled steel tubes (RACFSTs) conducted using grey relational evaluation and backpropagation (BP) neural networks. The results of the grey sensitivity analysis indicate that the effective water-to-cement ratio, steel tube strength grade, effective water-to-cement ratio, RA content, and axial load ratio are the most influential set of parameters on RACFSTs. BP neural networks were employed to estimate the load-carrying capacity of RACFSTs, and two simple expressions were proposed to model the RA content influence on the axial and lateral load-carrying capacities of RACFST columns. Pachideh and Golhaki, in 2020, assessed the concrete-filled steel tube column confined with fiber-reinforced polymers (FRP) experimentally and numerically. Three columns were tested under monotonic axial compressive loading and numerically analyzed using ANSYS software [15]. The ultimate capacity of each tested composite column was compared to the theoretical capacity of the proposed numerical model, demonstrating good compatibility and agreement between the experimental specimens and numerical analysis [16]. Pachideh et al. [17], in 2021, examined the temperature rise's impact on Concrete-Filled Double Skin Tubular Steel Columns with prismatic geometry. It examines columns with square, diamond, and circular interior cores and cyclic loads. Results show circular core columns experience more intensive damages, with diamond-shaped interior cores experiencing twice as much initial stiffness and ductility ratio. In 2020, Pachideh et al. [18] Experimentally investigated the cyclic performance of the geometrically prismatic concrete filled double-skin steel tubular (CFDST) columns. They studied the seismic performance of concrete-filled double-skin steel tubular columns with prismatic geometry. Results show that the failure mode of columns with an inner section of square or diamond is similar, but those with circular sections incur more intense damages. The initial stiffness and ductility ratio of diamond-shaped columns is greater than other columns. A steel beam to concrete-filled double-skin steel tubular (CFDST) column joint was developed to improve the widespread use of CFDST columns in buildings, in 2022, by Fan et al. [19]. Comparative studies of six specimens under pseudo-static cyclic tests revealed excellent ductility and improved seismic indices. Bolt diameter increased bearing capacity, ductility, and energy dissipation, but decreased ductility and energy dissipation. Concrete fill degree increased bearing capacity but decreased ductility and energy dissipation. Calculation model of initial rotational stiffness proposed. In 2023, Jin et al. [20] investigated the stiffening of thin-walled LHR-CFDST columns under axial compression. The test results showed that the stiffened measures effectively delayed local buckling and increased the peak load. Finite element models were applied to the mechanical mechanism analysis to improve the confinement of the inner and outer steel tubes and the ultimate strength of the concrete.

Buckling is one of the most important phenomena that occur when a slender structural component, such as a column or beam, fails under compressive loads. Therefore, the critical buckling load and buckling behavior of CFDST columns under compressive and torsional loads have been studied in various studies. the buckling of nine square concrete-filled box column (CFBC) specimens was tested and simulated with ABAQUS by Chen et al. [21]. Results showed

that horizontal arch action and vertical arch action provide significant confinement for concrete to gain and recover its strength. Hassanein et al. [22] studied the buckling behavior of CFDST columns, which consist of dual steel tubes with concrete filled in the entire tubular section. Their studies showed that intermediate and long CFDST columns fail by elastic-plastic buckling and elastic buckling respectively. The confinement of the external tubes also differs between intermediate and long CFDST columns, and using high-strength and ultra-high-strength concrete cores is not useful. The buckling behavior of axially loaded circular concrete-filled double-skin steel tubular short columns was studied by Ahmed et al. [23], they developed a numerical model to study the nonlinear performance of axially loaded short CFDST columns incorporating an accurate concrete confinement model. A novel expression is proposed to calculate lateral confining pressure and a reduction factor is suggested to accurately predict post-peak behavior. The accuracy of the model is verified against experimental tests and the applicability of existing design standards is verified. The research of Ipek et al. [24] has focused on square single-skin concrete-filled steel tubular (CFST) columns and elliptical concrete-filled double-skin steel tubular (CFDST) columns. A finite element (FE) method was used to investigate the axial compressive performance of elliptical CFDST short columns. Results showed that the generated FE model could be employed in the estimation of the behavior of elliptical CFDST short columns. Parametric studies revealed that the thickness of the outer steel tube, steel yield strength, concrete compressive strength, and aspect ratio of the elliptical section influence the performance of the elliptical CFDST short column. To enhance the comprehension of this paper, we propose the inclusion of a flowchart outlining the planned course of action. Figure 2.

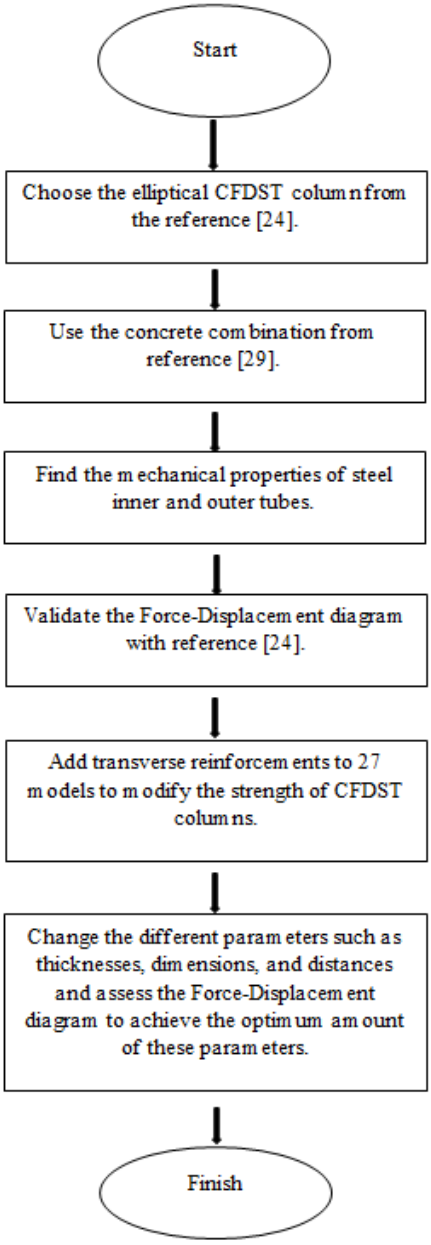

Fig 2. Structured and purposeful flowchart of the current study.

2. Validation

Based on the tests conducted on most of the models examined for the CFDST column, it has been observed that buckling often occurs in the outer tube section, which significantly reduces the columns' ability to support loads. To address this issue, our study proposes the utilization of transverse reinforcements installed on the exterior wall of these columns to enhance their load-bearing capacity.

We will conduct a parametric study on these transverse reinforcements to achieve this

objective using the finite element method implemented through Abaqus Software. This study will assess the impact of various parameters, such as thickness, dimensions, and distances, on the outer wall of elliptical CFDST columns. By analyzing these parameters, we aim to identify the optimal model that can maximize the increase in load-bearing capacity. Through the proposed parametric study, we intend to gain insights into the effectiveness of different configurations of transverse reinforcements in enhancing the overall performance of elliptical CFDST columns. This research has the potential to contribute to the development of more resilient structural designs that can withstand higher loads and mitigate the occurrence of buckling in the outer tube section. Therefore, the objective of this study is to investigate the impact of transverse reinforcements and their key parameters on the load-bearing capacity and buckling behavior of elliptical CFDST (Concrete Filled Steel Tube) columns. Initially, an elliptical column specimen from a reference paper [24] is analyzed using Abaqus software. The obtained results for the load-bearing capacity will be compared with the findings presented in this study to ensure the accuracy and reliability of the analysis.

Once the results are validated, transverse reinforcements will be incorporated into 27 models, positioned on the outer tube of the elliptical CFDST column. The parameters to be considered include the thickness, dimensions, and distances of these reinforcements. The objective is to investigate how these parameters influence the load-bearing capacity and buckling behavior of elliptical CFDST columns.

By conducting this comprehensive analysis, the study aims to contribute to the understanding of the role of transverse reinforcements and their effective parameters in enhancing the structural performance of elliptical CFDST columns.

In this research, the reference paper [24] including specimen E2 has been used to validate the results of a short CFDST column with an elliptical cross-section. The behavior of concrete and steel has changed due to the confinement of concrete from inside and outside by steel tubes which increases the strength and ductility of concrete. The behavior of steel tubes in this study has been considered bilinear elastic-plastic with isotropic stiffness, which was selected from the paper by Han [25]. Applying concrete inside the steel and confining it increases the strength and ductility and reduces the brittleness. The amount of confinement and its effect depends on the diameter-to-thickness ratio (D / t), and this effect can be neglected for ratios more than 150. In this research, the behavior of confined and unconfined concrete is presented with two different diagrams, which are presented in Figure 4, which include:

1. A region as the elastic zone (region O to A)
2- A region as the strain-hardening zone (region A to B)
3- A region as the strain-softening zone (region B to C) [26].

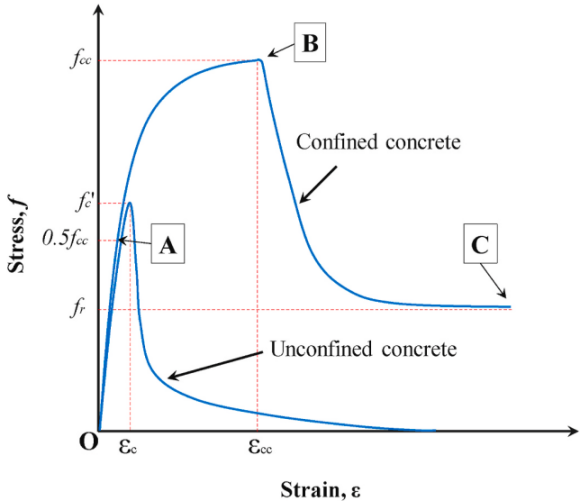

Fig 3. Stress-strain behavior of confined and unconfined concrete [26,27].

In Figure 3, *fc*, *fcc* and *fr* are the strength of unconfined concrete (80% of cubic concrete's strength), confined concrete's strength, and residual strength, respectively. Also, in this

diagram, εc and εcc are the strains corresponding to the compressive strength of unconfined and confined concrete, respectively. In this study, the amount of unconfined strain εc is 0.003 according to the ACI suggestion [28]. The modulus of elasticity of concrete is equal to 35.2 GPa and the Poisson's ratio is equal to 0.2. To define the behavior of concrete outside the elastic region, the Drager-Prager model has been used, the parameters of which have been extracted from the reference paper [28] and entered Abaqus software. The specimen analyzed in the validation section is an elliptical CFDST column with large diameters of the outer and inner tubes equal to 240 mm and 142 mm, respectively, and small diameters of the outer and inner tubes equal to 160 mm and 62 mm, respectively, thicknesses of the outer and inner tube equal to 3.62 and 3.72 mm, respectively and its length equal to 720 mm. A schematic of the cross-section of the validation specimen is provided in Figure 4.

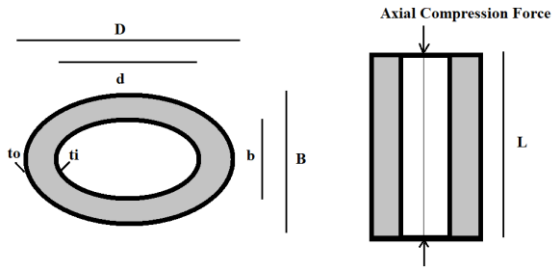

Fig 4. Schematic of the elliptical CFDST column geometry analyzed in the validation specimen.

To apply the load to the upper part of the column and to apply the boundary conditions to the lower part of the model, two endplates have been used. Tie constraint is used to connect the endplates to the inner and outer tubes. Also, a surface-to-surface contact constraint with a coefficient of friction of 0.6 has been used to connect the inner and outer tubes to the concrete surface. The same coefficient of friction between top and bottom endplates and concrete surfaces is used. To apply the boundary conditions to the top and bottom endplates, they are converted into two rigid bodies by selecting a reference point. The bottom endplate of the model is fully constrained while a displacement is applied to the top endplate of the model and the load-bearing capacity of the column is extracted from Abaqus software which will be presented in the results section. The element type of mesh used for different parts of the model is C3D8R. Mesh sensitivity analysis was conducted to determine the optimal meshing configuration. The mesh size was refined to 25 mm for the main regions of the model. To capture more accurate details, the peripheral areas, including the column and inner and outer tubes, were assigned a finer mesh with a size of 10 mm. Figure 5 illustrates a schematic representation of the resulting meshed model.

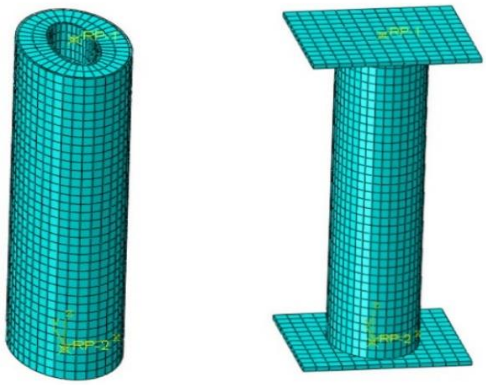

Fig. 5. Mesh of the validation model.

To evaluate mesh sensitivity, the initial mesh sizes used for the model and peripheral meshing of the samples were 200 mm and 40 mm, respectively. The samples were then analyzed, and the load-displacement diagram and load-bearing capacity were extracted and compared with a reference. However, significant differences were observed between the results obtained and the reference data. In order to reconcile these disparities, the mesh size was gradually reduced in subsequent iterations. The load-bearing capacity and corresponding results were extracted and compared at each step. This process was repeated until the desired maximum carrying capacity and load-displacement diagram, consistent with the reference article, was achieved. Eventually, by employing a mesh size of 25 mm for the model and a peripheral

mesh of 10 mm for the samples, the results obtained coincided with those of the reference article [24].

The reference [24] also investigated elliptic CFDST (Concrete-Filled Double-Skin Tubular) columns using Abaqus software. To validate their model, they compared the results with reference [29], which conducted laboratory work on CFDST elliptical columns. Since reference [24] was a numerical study, it did not provide specific details regarding the concrete mixture parameters. Therefore, reference [29] was utilized to obtain the concrete combination used in the study. The concrete combination employed in the reference [29] is as follows:

- Cement: 440 $^{kg}/_{m^3}$
- Blast furnace slag: 143 $^{kg}/_{m^3}$
- Water: 194 $^{kg}/_{m^3}$
- Sand: 683 $^{kg}/_{m^3}$
- Coarse aggregate: 855 $^{kg}/_{m^3}$
- Additional high-range water reducer (HRWR): 5.83 $^{kg}/_{m^3}$

These mixed proportions were employed in the numerical analysis conducted in reference [24] using Abaqus software. The results of this analysis were then compared with the experimental findings presented in reference [29]. The static analysis was employed for all the samples, In the Abaqus software, considering significant and non-linear shape changes. This type of analysis investigates the impacts of substantial shape variations within the model and acknowledges that material behavior is non-linear under certain conditions, particularly in cases of extreme loading. Linear approximations are inadequate to capture these non-linear behaviors accurately.

The mechanical properties related to the outer and inner steel pipe, concrete, and transverse reinforcements are presented in Table 1.

Table 1. Mechanical properties of materials used in this research [24].

Material type	Elasticity Module (MPa)	Poison ratio	Max Compressive Strength (GPa)	Yield Strength (GPa)	Ultimate Strength (GPa)
Concrete	35.2	0.2	65.5	-	-
Steel Inner Tube	200	0.3	-	380	471
Steel Outer Tube	200	0.3	-	319	434
Steel transverse reinforcements	200	0.3	-	319	434

2.1. Results of the validation

The results of the validation specimen analyzed here are presented in this section. The analyzed specimen was one of the models of the reference paper [24], which was analyzed to validate the research process. Results of the force-displacement diagram analyzed in this study, which was related to the E2 specimen of the reference paper [24], are presented in Figure 6.

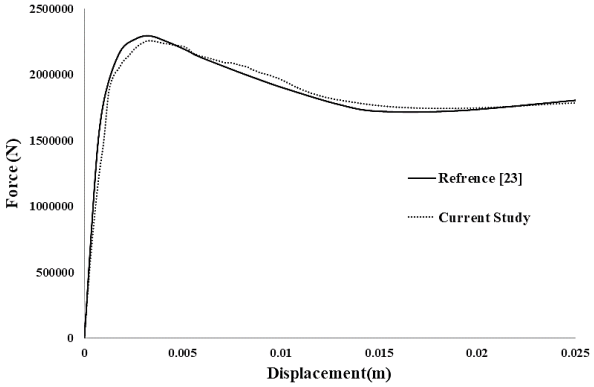

Fig 6. Comparison of the force-displacement diagram in reference paper [24] and of Abaqus analysis.

As can be seen in Figure 6, the results obtained from the Abaqus analysis are in good agreement with the results obtained from the reference [24], while a slight difference can be attributed to the meshing error, and since the error value is less than 5%, the results are acceptable.

The comparison between the results obtained from this research and reference [24] is presented in Table 2.

Table 2. Comparison of the obtained results from the current research with the reference article [24].

Research	in load-bearing capacity (KN)	Error Percentage with reference [24]
Current Research	2256	2.5%
Reference [24]	2315	-

It is important to note that the reference [24], used in this research, compared its results with the results obtained from the laboratory samples referenced in the article [29]. Therefore, the validation of the results from reference [24] was based on the laboratory data [29]. Consequently, the results of the current study also align with the experimental data from reference [29] in the section related to the CFDST column without an amplifier. Furthermore, this research not only compared an elliptic CFDST column with the data from the mentioned references but also introduced additional innovations. Specifically, transverse reinforcements were incorporated into the column, and the impact of these reinforcements on improving the column's behavior was investigated.

3. Models of the research

In this section, we provide the specifications of the analyzed models in this research. A total of 27 models were examined, where transverse reinforcements were added to the validation section specimens. The models were varied in terms of the thickness, dimensions, and spacing of these transverse reinforcements. All specimens were subjected to a similar loading condition as the validation section. Additionally, the mesh size and type used for the transverse reinforcements were the same as those employed for the outer tube of the CFDST column analyzed in the validation section. Table 3 presents the characteristics of the analyzed models in this research. The models are named using the letter "E" followed by five digits. The first two digits indicate the model number, the third digit represents the thickness of the transverse reinforcement in millimeters (mm), the fourth digit denotes the dimensions of the transverse reinforcements in centimeters (cm), and the fifth digit indicates the distance between the transverse reinforcements in centimeters (cm).

For instance, model E01422 corresponds to Model No. 1 with a transverse reinforcement thickness of 4 mm, dimensions of 2 cm, and 2 cm between the reinforcements. The percentage of transverse reinforcements is determined by calculating the ratio between the area covered on the outer surface of the CFDST column and the area of the reinforcements. The values corresponding to these percentages are provided in Table 3.

Figure 7 depicts the schematic of models 1 to 3, illustrating the transverse reinforcement with 2 cm and dimensions of 2, 4, and 6 cm. Similarly, Figure 8 showcases models 4, 5, and 6 with reinforcement having 4 cm and dimensions of 2, 4, and 6 cm. Finally, Figure 9 displays models 7, 8, and 9, featuring reinforcement with 6 cm and dimensions of 2, 4, and 6 cm.

Table 3. Specifications of 27 models.

Model name	Model short name	The thickness of transverse reinforcements (mm)	Dimension of transverse reinforcements (mm)	Distance between transverse reinforcements (mm)	Percentage of transverse reinforcements (%)
Model No. 1	E01422	4	2	2	50%
Model No. 2	E02442	4	4	2	66%
Model No. 3	E03462	4	6	2	75%
Model No. 4	E04424	4	2	4	33%
Model No. 5	E05444	4	4	4	50%
Model No. 6	E06464	4	6	4	60%
Model No. 7	E07426	4	2	6	25%
Model No. 8	E08446	4	4	6	38%
Model No. 9	E09466	4	6	6	50%
Model No. 10	E10622	6	2	2	50%
Model No. 11	E11642	6	4	2	66%
Model No. 12	E12662	6	6	2	75%
Model No. 13	E13624	6	2	4	33%
Model No. 14	E14644	6	4	4	50%
Model No. 15	E15664	6	6	4	60%
Model No. 16	E16626	6	2	6	25%
Model No. 17	E17646	6	4	6	38%
Model No. 18	E18666	6	6	6	50%
Model No. 19	E19822	8	2	2	50%
Model No. 20	E20842	8	4	2	66%
Model No. 21	E21862	8	6	2	75%
Model No. 22	E228624	8	2	4	33%
Model No. 23	E23844	8	4	4	50%
Model No. 24	E24864	8	6	4	60%
Model No. 25	E25826	8	2	6	25%
Model No. 26	E26846	8	4	6	38%
Model No. 27	E27866	8	6	6	50%

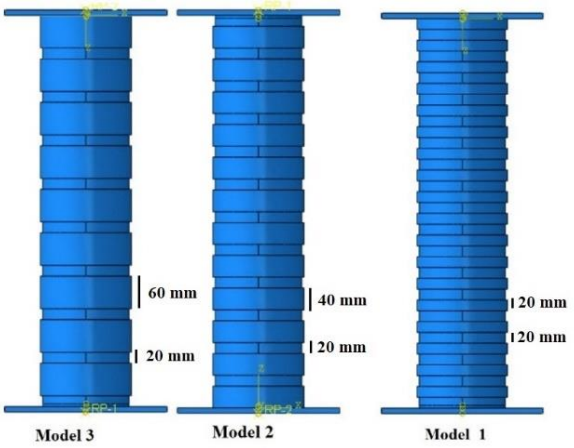

Fig 7. Models 1, 2, and 3 with 2 cm reinforcements (dimensions of 2, 4, and 6 cm) and thickness of 4 mm.

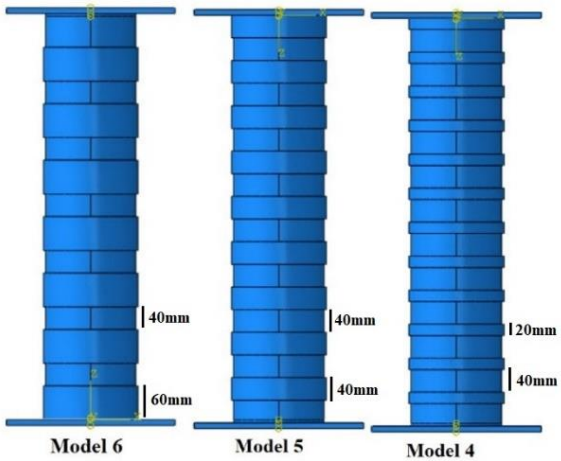

Fig 8. Models 4, 5, and 6 with 4 cm reinforcements (dimensions of 2, 4, and 6 cm) and thickness of 4 mm.

The geometry of models 10 to 18 and 19 to 27 is like models 1 to 9, while the only difference is the thickness of the transverse reinforcements which has changed from 4 mm to 6 and 8 mm. All models, similar to the validation, are subjected to compression loading of the displacement control type, and the load-bearing capacity and deformations associated with 27 models are extracted from the software, which will be presented in the result section.

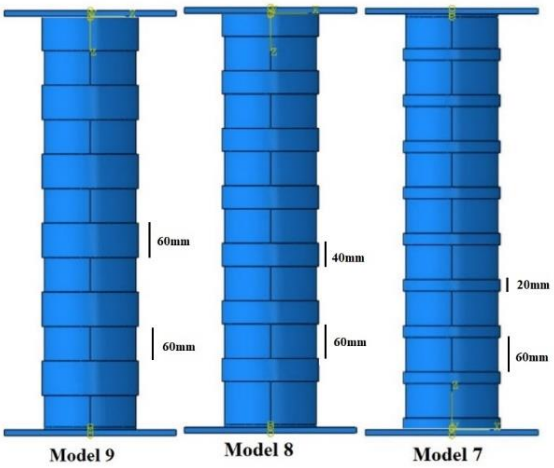

Fig 9. Models 7, 8, and 9 with 6 cm reinforcements (dimensions of 2, 4, and 6 cm) and thickness of 4 mm.

4. Results and discussion

In this section, the results obtained from 27 models analyzed in this paper are presented. In models, transverse reinforcements with different thicknesses, dimensions, and distances, the specifications of which are presented in Table 3, are placed on the CFDST elliptical column, and analyzed in the validation section to investigate their effect on the force-displacement diagram (load-bearing capacity), buckling behavior and ultimate strength in these columns.

4.1. Results of the force-displacement

In the 27 models investigated in this study, which were analyzed in Abaqus software, all specimens were subjected to the same displacement. In other words, displacement control analysis is used, and force-displacement diagrams are presented and compared with each other in this section. Figure 10 displays force-displacement diagrams for 4mm reinforcements in models 1-9. In these diagrams, the status of each graph is represented by an expression, for example, "1_E01422_t = 4mm_d = 2cm_di = 2cm". This expression contains a number that indicates the model number, for example, here 1 represents model 1. The expression E01422 in this term indicates the abbreviation of the model, which is presented in Table 3. The expression t = 4mm indicates the thickness of the transverse reinforcements and the expressions d = 2cm and di = 2cm indicate the dimensions of the transverse reinforcements and the distance between them, respectively. As shown in Figures 10(a), 10(b), and 10(c), by increasing the dimensions of the transverse reinforcements from 2 to 4 and 6 cm, at equal thicknesses and distances, the load-bearing capacity in the specimens increases and the reason for this can be related to the increase in the area and volume of reinforcements, which also increase the amount of stiffness and strength of the structure and as a result, load-bearing capacity in them are also improved. The noteworthy point in all these diagrams compared to the diagram presented in Figure 5, is that they have not buckled, due to the use of transverse reinforcement, and this has led to preventing the reduction in load-bearing capacity in the specimens compared to the validation. In the following, a force-displacement diagram of the specimens having reinforcements with a thickness of 6 mm and various dimensions and distances is presented according to the results obtained in Figure 11, in this group of models, the amount of load-bearing capacity in the specimens in all three categories is similar to the previous category presented in Figure 10.

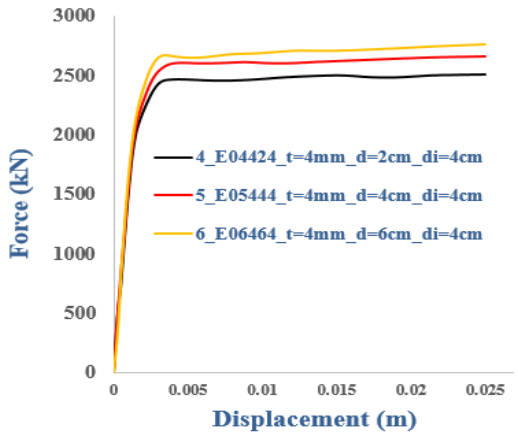

(a)

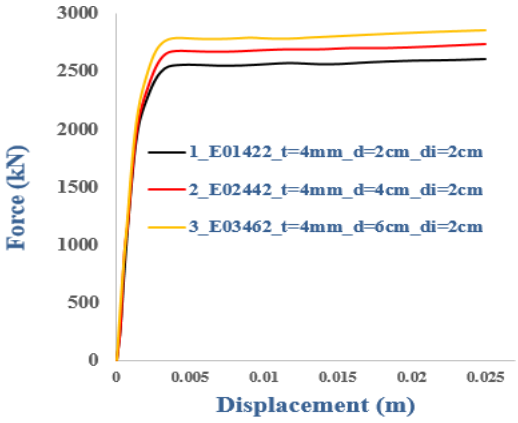

(b)

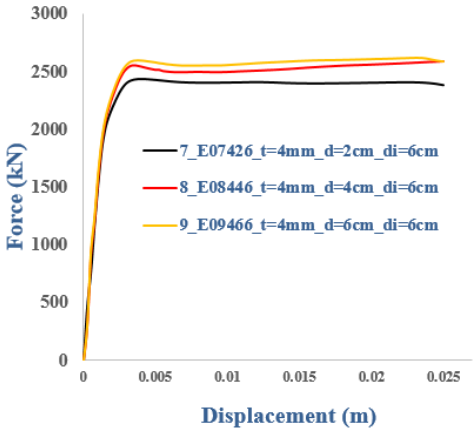

(c)

Fig 10. The force-displacement diagram in models 1 to 9 (thickness 4 mm and various distances and dimensions of transverse reinforcements).

With increasing the dimensions of the transverse reinforcements in all three categories and at different distances, the amount of load-bearing capacity has increased, but with increasing distances from 2 to 4 and 6 cm in Figure 11(a), to 11(b) and 11(c), and with increasing transverse reinforcement dimensions, increasing intensity of load-bearing capacity has been reduced. In other words, the effect of dimensions on transverse reinforcements will be reduced at longer distances, and the reason for this can also be

attributed to the interaction effects that the reinforcements have on each other and by increasing the distance between them, the intensity of these effects decreases while rising the dimensions shows less effect on increasing the load-bearing capacity. In the following, force-displacement diagrams are presented in specimens with a thickness of 8 mm and different dimensions and distances analyzed in models 19 to 27.

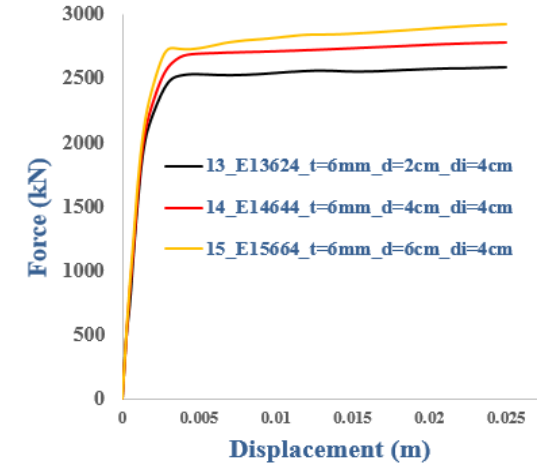

(a)

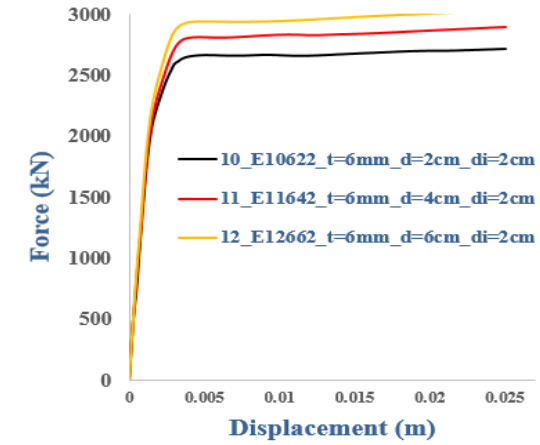

(b)

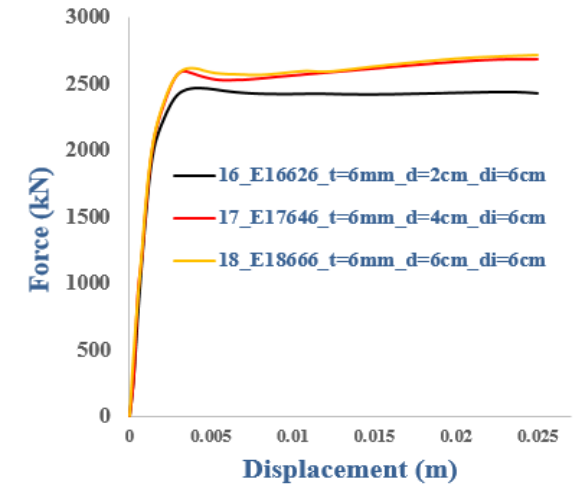

(c)

Fig 11. The force-displacement diagram in models 10 to 18 (thickness 6 mm and various distances and dimensions of transverse reinforcements).

As can be seen in Figure 12, in this category, a rise in dimensions in models 19, 20, and 21, with a distance of 2 cm and equal thickness, will increase load-bearing capacity significantly, and with increasing distance between the specimens in the second and third categories, which are presented in Figures 12(a), 12(b) and 12(c), the intensity of increasing load-bearing capacity has been reduced, and especially in the third category, the vertical distance between the two diagrams is sharply reduced. The difference between the two diagrams is lowered, and the reason for this can also be attributed to the reduction of the effects of the reinforcements by increasing the distance. In general, the result that can be obtained from Figures 10, 11, and 12 is that by using transverse reinforcements in addition to preventing buckling in the structure and delaying it, load-bearing capacity in elliptical CFDST columns will also be improved and deterioration of load-bearing capacity is reduced due to buckling in the specimens. Also, by increasing the distance between the reinforcements, due to the reduction of interactions, although their dimensions rise, the intensity of increasing load-bearing capacity in the specimens is reduced. In the following, a force-displacement diagram is presented in specimens with dimensions of 2 cm and with various distances and thicknesses between them to determine the effects of distance change in equal thicknesses.

In Figure 13, the results of the force-displacement diagram in specimens with dimensions of 2 cm and variable distances in equal thicknesses are presented in three categories. In the first group which is in Figure 13(a), the thickness of the specimens is equal to 4 mm and only distances between the specimens have changed. In the second group which is in Figure 13(b), the thickness is equal to 6 mm and the distance between the specimens has been varied in the third category, which is presented in Figure 13(c), like the previous two categories, only the thickness has changed to 8 mm. The distances between the specimens have changed between 2, 4, and 6 cm in equal dimensions of 2cm. The results obtained from these three diagrams presented in Figure 13 show that by increasing the distances between the specimens in equal thickness, load-bearing capacity will decrease by a relatively linear trend and the reason for this can be attributed to the reduction of stiffness and strength in the specimens due to the increase in the distance between the reinforcements, which causes the strength of the specimens to the applied loads to lower and load-bearing capacity to decrease linearly with increasing distance.

In the following, force-displacement diagrams are presented in specimens 1, 10, and 19, which had transverse reinforcements with equal dimensions and distances, and only their thickness was changed to show the effect of changes in the thickness on the force-displacement diagram.

According to the results obtained from Figure 14, with increasing thickness in transverse reinforcements, load-bearing capacity in the specimens has increased linearly and it can be said that the thickness changes on increasing load-bearing capacity in different specimens are linear. Because the trend of changing the results was similar in terms of thickness in different models, only comparisons were made between three specimens with different thicknesses.

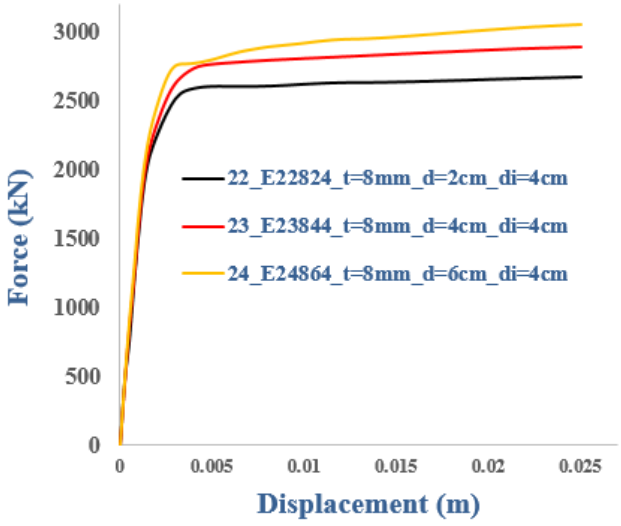

(a)

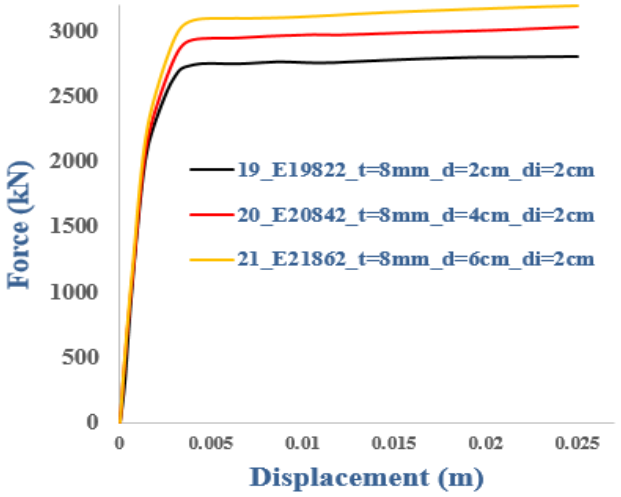

(b)

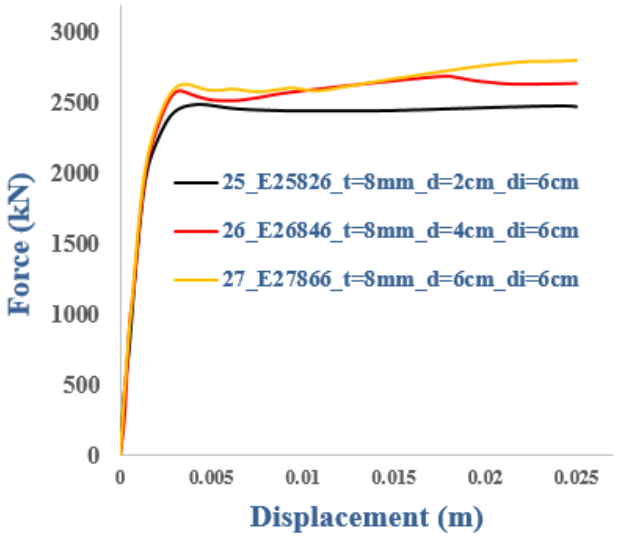

(c)

Fig 12. The force-displacement diagram in models 19 to 27 (thickness 8 mm and various distances and dimensions of transverse reinforcements).

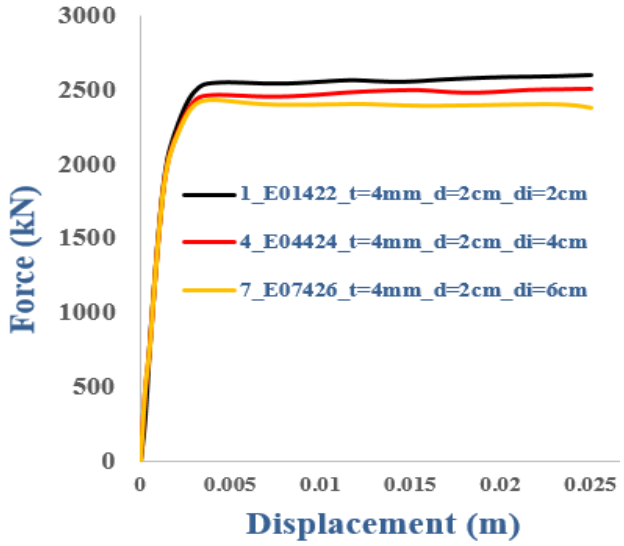

(a)

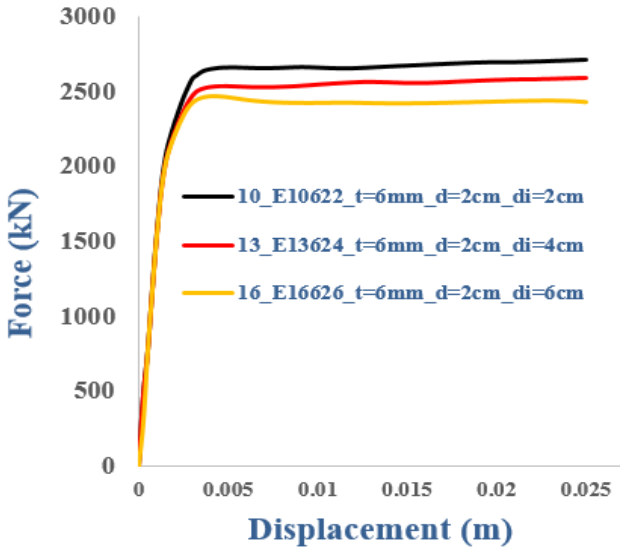

(b)

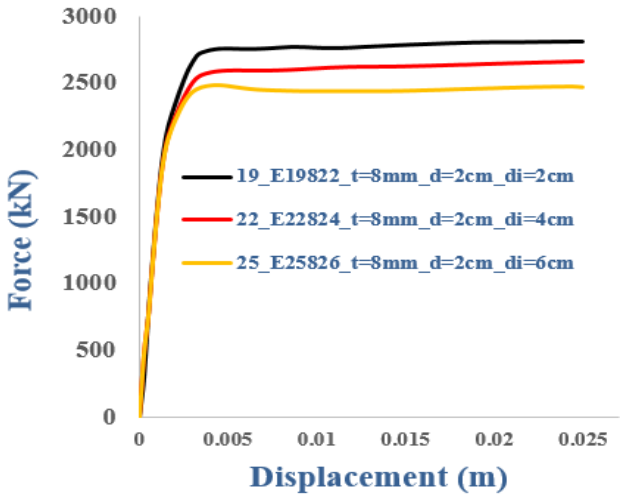

(c)

Fig 13. The force-displacement diagram in models with dimensions of 2 cm (various thicknesses and distances of transverse reinforcements).

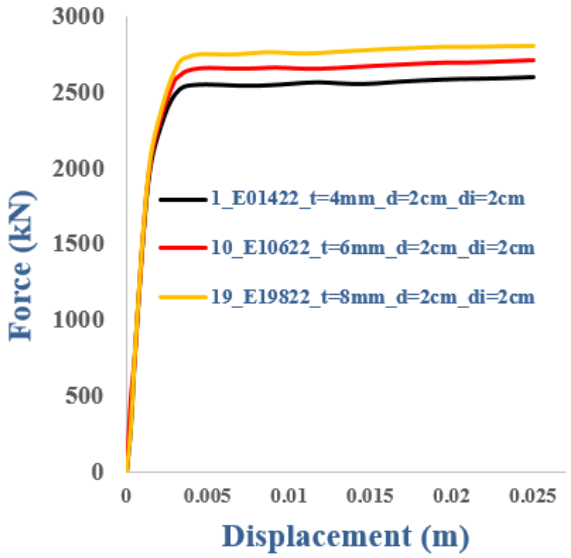

Fig 14. The force-displacement diagram in models with variable dimensions (constant thickness and distance between transverse reinforcements).

4.2. Maximum axial strength

In this section, the results related to the maximum axial strength in each specimen along with ductility are presented. The maximum axial strength is derived from the obtained force-displacement diagram for each specimen, which is presented in Table 4.

A comparison of the maximum axial strength diagram in 27 specimens is presented as a bar diagram in three categories in Figures 15, 16, and 17. In the first category, the results are related to models 1 to 9, in which the thickness of the transverse reinforcements is equal to 4 mm. Results for the next category are for models 10 to 18, in which the thickness of the transverse reinforcements has changed from 4 to 6 mm. In the third category, models 19 to 27, the thickness of the transverse reinforcements has finally changed to 8 mm. In each category, in the first to third specimens, the distance is equal to 2 cm and their dimensions vary between 2, 4, and 6 cm.

As shown in Figure 15, the maximum load-bearing capacity in models 1 to 3 increased by 9.4% when dimensions rise from 2 to 4 and 6 cm, and the distance between them is equal to 2 cm. This increase was 9.3% in specimens 4 to 6, where the distance between the reinforcements was 4 cm, and in specimens 7 to 9, where the distance between the specimens was 6 cm, it was 6.2%. As can be seen, by increasing the distance between the reinforcements, the effect of raising their dimensions on the maximum axial strength in the models is reduced, and the reason for this is to reduce the effects of reinforcements by increasing the distance between them and more spread of failure within the specimens.

Table 4. Maximum axial strength.

Model name	Model abbreviated name	The maximum amount of axial strength (kN)
Model No. 1	E01422	2548
Model No. 2	E02442	2689
Model No. 3	E03462	2790
Model No. 4	E04424	2474
Model No. 5	E05444	2620
Model No. 6	E06464	2705
Model No. 7	E07426	2437
Model No. 8	E08446	2538
Model No. 9	E09466	2589
Model No. 10	E10622	2697
Model No. 11	E11642	2817
Model No. 12	E12662	2976
Model No. 13	E13624	2549
Model No. 14	E14644	2722
Model No. 15	E15664	2823
Model No. 16	E16626	2490
Model No. 17	E17646	2561
Model No. 18	E18666	2605
Model No. 19	E19822	2702
Model No. 20	E20842	2884
Model No. 21	E21862	3076
Model No. 22	E228624	2615
Model No. 23	E23844	2768
Model No. 24	E24864	2876
Model No. 25	E25826	2474
Model No. 26	E26846	2622
Model No. 27	E27866	2701

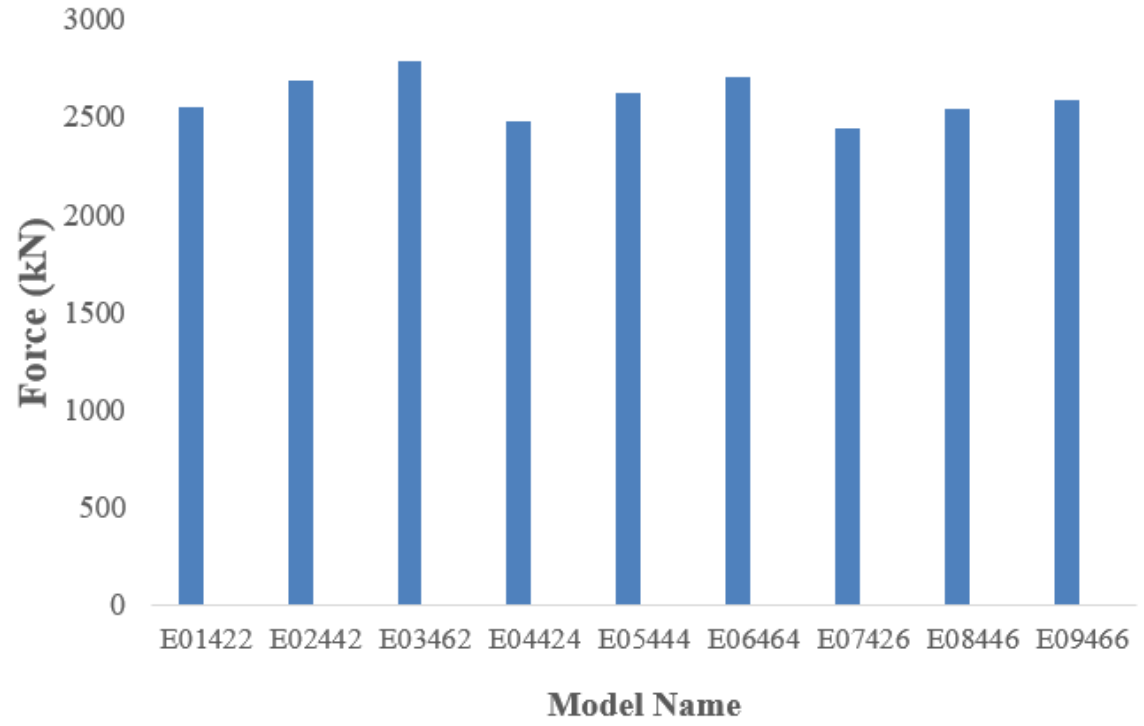

Fig 15. Comparison of the maximum axial strength in models 1 to 9 with 4mm-thick reinforcements.

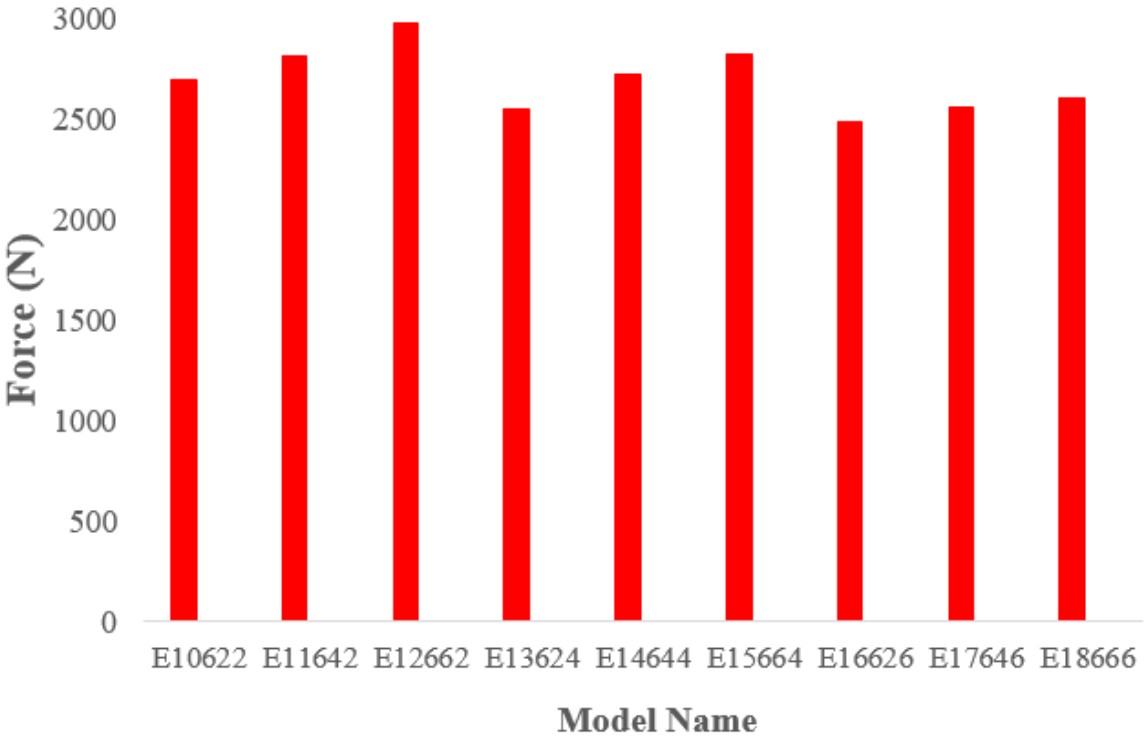

Fig 16. Comparison of the maximum axial strength in models 10 to 18 with 6mm-thick reinforcements.

According to the results obtained from Figure 16, the amount of increase in the maximum value of axial strength in models 10 to 12, in which dimensions have increased from the value of 2 to 6 cm at a distance of 2 cm, was 10.3% while it is 10.7% in specimens 13 to 15, which have a distance of 4 cm. On the other hand, the increase of the maximum axial strength in specimens 16 to 18 with a distance of 6cm in between is equal to 4.6%.

Fig 17. Comparison of the maximum axial strength in models 19 to 27 with 8mm-thick reinforcements.

The results of comparing the maximum axial strength in models 19 to 27 are shown in Figure 17. According to the obtained results, the percentage of increase of the maximum axial strength is equal to 13.8% in models 19 to 21, which had a distance of 2 cm, while it is equal to 10% in models 22 to 25, which had a distance of 4 cm, and finally is 8% for models 25 to 27 with a distance of 6cm.

4.2. Disadvantages of CFDST columns

Although the CFDST columns have a high Strength-to-Weight ratio, high axial load capacity, structural stability, constructability, and high Fire Resistance, the disadvantages of CFDST columns and seeds should be discussed in more detail.

CFDST (Confined Fiber-reinforced concrete-filled Steel Tube) columns and seeds are commonly used in structural engineering, but they do have some disadvantages, including:

1. Cost: CFDST columns and seeds can be more expensive than traditional reinforced concrete or steel columns due to the use of specialized materials and construction techniques.
2. Difficulty in inspection: It can be challenging to inspect the internal condition of CFDST columns and seeds, which may cause problems with maintenance and repair in the long term.
3. Corrosion: While the steel tube provides excellent corrosion protection, it is still susceptible to corrosion over time, which can lead to a reduction in the structural integrity of the column.
4. Brittle failure: CFDST columns and seeds may experience brittle failure under severe loading conditions, which can be problematic for the safety of the structure.

5. Conclusion

In this study, the compressive strength and load-bearing capacity of elliptical CFDST columns reinforced with transverse reinforcements were investigated. For this purpose, an elliptical CFDST column was validated in Abaqus Software. After validating, transverse reinforcements were added to the elliptical CFDST column and parameters such as thickness, dimensions, and distance

between these transverse reinforcements were changed and the force-displacement diagram as well as the maximum axial strength in the specimens were extracted from these models, and then compared with each other. The results obtained from this study can be summarized as follows:

1. The finite element method with Abaqus Software was used to simulate the models and validation specimens in this research, whose results for the force-displacement diagram manifested a very good agreement with the result from the reference paper [24].
2. The amount of load-bearing capacity in all 27 models analyzed increased from 15 to 40% compared to the validation specimen without transverse reinforcement. In addition, due to the absence of buckling, load-bearing capacity in the specimens with transverse reinforcement did not decrease much after reaching the maximum strength, but in the validation, after reaching the maximum axial strength, load-bearing capacity reduced sharply when associated with displacement rise.
3. With increasing the thickness in transverse reinforcements from 4 to 6 and 6 to 8 mm, load-bearing capacity and the maximum amount of axial strength increased up to 20% in all similar models and with different thicknesses. Variations of load-bearing capacity and maximum compressive strength of the specimens were almost linear with changing thickness.
4. With increasing dimensions of transverse reinforcements from 2 to 4 and from 4 to 6 cm in all similar specimens with the same thickness and distances, load-bearing capacity and maximum compressive strength increased up to 15%. In this situation, by rising dimensions of the reinforcements, the ascending intensity of load-bearing capacity and the maximum axial strength in the specimens were reduced, while the highest increase in the models with dimensions change from 2 to 4 cm was much more outstanding than the specimens where dimensions changed from 4 to 6 cm.
5. By increasing the distance between the reinforcements from 2 to 4 and from 4 to 6cm, the load-bearing capacity in the specimens decreased to 10%. The results obtained from the analysis showed that by increasing distances between the specimens in equal thickness, load-bearing capacity will decrease with a relatively linear trend where the reason for this can be attributed to reduced stiffness and strength in the specimens due to increasing distance between the reinforcements. This leads to the fact that the strength of the specimens to the applied loads is reduced, and load-bearing capacity decreases linearly with rising distance.

Funding

This work was not funded by any organizations.

Conflicts of interest

The authors declare that they have no known competing financial interests or personal relationships that could have appeared to influence the work reported in this paper.

Authors contribution statement

Ali Mohammad Ali: Conceptualization, Data analysis.

Sima Besharat Ferdosi: Data analysis and Draft Preparation, Reviewing and Editing.

Laith Kareem Obeas: Data analysis, Simulation.

Alwaleed Khalid Ghalib: Data analysis and Draft Preparation.

Meisam Porbashiri: Simulation, Reviewing and Editing.

References

[1] Sulthana UM, Jayachandran SA. Axial compression behaviour of long concrete filled double skinned steel tubular columns. Structures, vol. 9, Elsevier; 2017, p. 157–64.

[2] Elchalakani M, Patel VI, Karrech A, Hassanein MF, Fawzia S, Yang B. Finite element simulation of circular short CFDST columns under axial compression. Structures, vol. 20, Elsevier; 2019, p. 607–19.

[3] Yan X-F, Zhao Y-G. Compressive strength of axially loaded circular concrete-filled double-skin steel tubular short columns. J Constr Steel Res 2020;170:106114.

[4] Ahmed M, Liang QQ, Patel VI, Hadi MNS. Local-global interaction buckling of square high strength concrete-filled double steel tubular slender beam-columns. Thin-Walled Struct 2019;143:106244.

[5] Hu H-T, Su F-C. Nonlinear analysis of short concrete-filled double skin tube columns subjected to axial compressive forces. Mar Struct 2011;24:319–37.

[6] Ferdosi SB. Thermal effect on the post-buckling and mechanical response of single-walled carbon nanotubes: A numerical investigation. Mech Eng 2022;9:1–6.

[7] Lai MH, Song W, Ou XL, Chen MT, Wang Q, Ho JCM. A path dependent stress-strain model for concrete-filled-steel-tube column. Eng Struct 2020;211. https://doi.org/10.1016/j.engstruct.2020.110312.

[8] Rahimighazvini H, Masali MH, Saeidi S, Barzegaran R. Disaster impact prediction in the power grid using artificial intelligence based on Texas synthetic grid data replication. World J Adv Res Rev 2024;21:1631–41.

[9] Alvansazyazdi M, Figueroa J, Paucar A, Robles G, Khorami M, Bonilla-Valladares PM, et al. Nano-silica in Holcim general use cement mortars: A comparative study with traditional and prefabricated mortars. Adv Concr Constr 2024;17:135.

[10] Le TT, Patel VI, Liang QQ, Huynh P. Numerical modeling of rectangular concrete-filled double-skin steel tubular columns with outer stainless-steel skin. J Constr Steel Res 2021;179:106504. https://doi.org/10.1016/j.jcsr.2020.106504.

[11] Ye Y, Yao X-H, Guo Z-X. Performance of concrete-filled stainless steel tubes subjected to concentric tension: Numerical investigation and parametric study. Structures, vol. 32, Elsevier; 2021, p. 2222–31.

[12] Li M, Zong Z, Hao H, Zhang X, Lin J, Liao Y. Post-blast performance and residual capacity of CFDST columns subjected to contact explosions. J Constr Steel Res 2020;167:105960. https://doi.org/10.1016/j.jcsr.2020.105960.

[13] Arbabkhah H, Sedaghat A, Jafari Kang M, Hamidi M. Automatic Identification System-Based Prediction of Tanker and Cargo Estimated Time of Arrival in Narrow Waterways. J Mar Sci Eng 2024;12:215.

[14] Xu J, Wang Y, Ren R, Wu Z, Ozbakkaloglu T. Performance evaluation of recycled aggregate concrete-filled steel tubes under different loading conditions: Database analysis and modelling. J Build Eng 2020;30:101308. https://doi.org/10.1016/j.jobe.2020.101308.

[15] Doranga S, Ferdowsi SB, Li Y, Khanal M. A novel approach of fatigue testing and evaluation of electronic systems based on phase tracking. Microelectron Reliab 2024;155:115368.

[16] Pachideh G, Gholhaki M. Evaluation of concrete filled steel tube column confined with FRP. J Test Eval 2020;48:4343–54.

[17] Pachideh G, Gholhaki M, Moshtagh A. An experimental study on cyclic performance of the geometrically prismatic concrete-filled double skin steel tubular (CFDST) columns. Iran J Sci Technol Trans Civ Eng 2021;45:629–38.

[18] Pachideh G, Gholhaki M, Moshtagh A. Impact of temperature rise on the seismic

performance of concrete-filled double skin steel columns with prismatic geometry. J Test Eval 2021;49:2800–15.

[19] Fan J, Zhao J, Zhu Q, Ni Z, Liu J. Seismic behavior and analytical model for a fully bolted joint between CFDST columns and steel beams. Structures, vol. 42, Elsevier; 2022, p. 515–30.

[20] Jin K-Y, Zhou X-H, Wen H, Deng R, Li R-F, Wang Y-H. Compressive behaviour of stiffened thin-walled CFDST columns with large hollow ratio. J Constr Steel Res 2023;205:107886.

[21] Chen C-C, Ko J-W, Huang G-L, Chang Y-M. Local buckling and concrete confinement of concrete-filled box columns under axial load. J Constr Steel Res 2012;78:8–21.

[22] Hassanein MF, Elchalakani M, Patel VI. Overall buckling behaviour of circular concrete-filled dual steel tubular columns with stainless steel external tubes. Thin-Walled Struct 2017;115:336–48.

[23] Ahmed M, Ci J, Yan X-F, Lin S, Chen S. Numerical modeling of axially loaded circular concrete-filled double-skin steel tubular short columns incorporating a new concrete confinement model. Structures 2021;30:611–27. https://doi.org/10.1016/j.istruc.2021.01.044.

[24] İpek S, Erdoğan A, Güneyisi EM. Compressive behavior of concrete-filled double skin steel tubular short columns with the elliptical hollow section. J Build Eng 2021;38:102200.

[25] Han L-H, Huo J. Concrete-filled hollow structural steel columns after exposure to ISO-834 fire standard. J Struct Eng 2003;129:68–78.

[26] Hu H-T, Huang C-S, Wu M-H, Wu Y-M. Nonlinear analysis of axially loaded concrete-filled tube columns with confinement effect. J Struct Eng 2003;129:1322–9.

[27] Binici B. An analytical model for stress–strain behavior of confined concrete. Eng Struct 2005;27:1040–51.

[28] Mander JB, Priestley MJN, Park R. Theoretical stress-strain model for confined concrete. J Struct Eng 1988;114:1804–26.

[29] Han L-H, Ren Q-X, Li W. Tests on stub stainless steel–concrete–carbon steel double-skin tubular (DST) columns. J Constr Steel Res 2011;67:437–52.